Quasi-analytic study of scattering from optical plasmonic patch antennas

Cristian Ciracì, J. Britt Lassiter, Antoine Moreau, and David R. Smith

Citation: J. Appl. Phys. **114**, 163108 (2013); doi: 10.1063/1.4827185
View online: http://dx.doi.org/10.1063/1.4827185
View Table of Contents: http://jap.aip.org/resource/1/JAPIAU/v114/i16
Published by the AIP Publishing LLC.

Quasi-analytic study of scattering from optical plasmonic patch antennas

Cristian Ciracì, J. Britt Lassiter, Antoine Moreau, and David R. Smith
Department of Electrical and Computer Engineering, Center for Metamaterials and Integrated Plasmonics, Duke University, Box 90291 Durham, North Carolina 27708, USA

(Received 25 August 2013; accepted 10 October 2013; published online 31 October 2013)

We present an analytical treatment of the optical scattering from film-coupled nanocubes. Film-coupled nanoparticles are a convenient platform for the demonstration of a variety of fundamental plasmonic phenomena, including nonlocality and field enhancement, and can also serve as the basis for controlled reflectance surfaces. The nanocube geometry is particularly amenable to analysis, since the cubes behave in large part as plasmon resonant patch antennas, allowing the well-known patch antenna equations to be applied with some modifications. In particular, we make use of the plasmon dispersion relation to avoid direct calculation of the effective inductance per unit length—which would include kinetic inductance contributions—instead calculating the effective waveguide mode index to incorporate plasmonic contributions. We compare the analytically derived field enhancement and spectral characteristics of the film-coupled nanoparticles with those obtained from full-wave finite-element simulations. © *2013 AIP Publishing LLC*. [http://dx.doi.org/10.1063/1.4827185]

I. INTRODUCTION

Certain configurations of metallic and other conducting nanoparticles that support surface plasmons can produce highly localized and strongly enhanced fields when illuminated with light. Field enhancement serves as the key mechanism in numerous optical phenomena of great interest, including surface enhanced Raman scattering,[1,2] enhanced fluorescence,[3] enhancement of nonlinearity,[4] sensing,[5] and many light generation or amplification schemes.[6–10] A larger field enhancement can directly translate to a more significant role for the associated phenomenon.

The largest field enhancements occur in nanosystems that have sharp, nanoscale protrusions, or in composites with nanoscale gaps between particles.[11–13] Thus, fully leveraging field enhancement requires nanoparticle configurations for which critical features can be controlled reproducibly to the sub-nanometer scale. Though early on such control was difficult to achieve, in recent years considerable progress has been made in the fields of nanolithography and colloidal synthesis, such that devices based on enhancement effects are becoming feasible.

A system of particular interest is that of the film-coupled nanoparticle, in which a nanoparticle positioned above a metal film couples to its electromagnetic image formed by the interaction of the nanoparticle and film.[14–19] The electromagnetic scattering properties of the film-coupled nanoparticle are very similar to those of a doublet—two closely spaced, interacting nanoparticles—a frequently studied archetypical system known to exhibit exceptionally large field enhancements.[20–23] In contrast to the doublet, however, the film-coupled nanoparticle system can be fabricated relatively simply by lithographic patterning or colloidal "bottom up" synthesis. Starting with a metal film, a dielectric spacer layer with precisely controlled thickness can be deposited using a variety of surface chemistries or atomic layer deposition (ALD). Nanoparticles placed on the dielectric layer are therefore spaced a uniform and tightly controlled distance from the film, such that the enhancement expected from the interaction is uniform and reproducibly at the single nanoparticle level. Film-coupled nanoparticles have been used to demonstrate 100% yield in surface-enhanced Raman experiments,[24] enhance catalysis,[25] and even probe the nonlocal metal response that occurs under the most extreme coupling conditions[26] (gaps smaller than one nanometer).

In a recent study, film-coupled nanocubes were used to form a surface with controlled reflectivity.[27] The electromagnetic properties of a film-coupled nanocube, nanodisk, or other planar particle are distinct from that of a film-coupled nanosphere, in that a transmission line mode can be formed between the film and the planar nanoparticles. This transmission line mode can undergo a geometrical resonance caused by reflections from the edges of the particle, leading to large local field enhancements and large scattering that depend on the geometry of the gap. For very small nanometer sized gaps between the nanocube and film, the localized field is nearly uniform across the gap and close to transverse electromagnetic (TEM) in character; thus, the film-coupled nanocube is, in fact, very similar to the well-known patch antenna ubiquitous in microwave technology. The large local enhancements and strong scattering associated with optical patch antennas recently motivated their use to enhance single photon emission.[28,29]

In this paper, we develop an analytical model of the film-coupled nanocube resonator, arriving at closed form expressions for the local field enhancement and scattering properties. Combining a transmission line model modified by the plasmon dispersion relation with results from the theory of patch antennas, we determine the coupling of an incident plane wave to the film-coupled nanoparticle—referred to as an optical patch antenna in the following—determining the resulting mode properties within the gap and expected radiation patterns. Reasonable approximations are introduced to enable the closed form expressions that

illustrate the dependencies of the various quantities of interest. We conclude by comparing the expected field enhancement and spectral properties with those obtained from full-wave simulations. Our conclusion is that the optical patch antenna can be analyzed in a manner similar to that of conventional radio-frequency (RF) patch antennas, with the main modification being for the plasmon dispersion relation associated with the metal-insulator-metal gap plasmon.[30] The effect of the gap plasmon is that the effective per length inductance is increased substantially due to kinetic inductance.[31] The increased inductance leads to a large effective propagation constant within the gap—equivalently, a large effective waveguide index—so that the optical patch at resonance is inherently much smaller relative to the wavelength than a microwave patch at resonance.

II. SUMMARY OF PATCH ANTENNA MODES

We first recall the properties of a conventional (RF) resonant patch antenna relevant for the ensuing analysis. A key simplifying assumption in the analysis of the resonant patch is that the boundary conditions at the four slots can be approximated as perfect magnetic conductors, with perfect electric conductors approximating the metal conductor on top and bottom of the patch. We consider a square patch, of height h and whose width and length are $W = L$, respectively. With respect to Figure 1, the imposition of these boundary conditions leads to the following conditions for the wave vector components:

$$\begin{aligned} k_x &= \frac{p\pi}{h} \quad p = 0,\ 1,\ 2,\ \ldots \\ k_y &= \frac{m\pi}{W} \quad m = 0,\ 1,\ 2,\ \ldots \\ k_z &= \frac{n\pi}{L} \quad n = 0,\ 1,\ 2,\ \ldots . \end{aligned} \tag{1}$$

We concentrate here on modes for which the electric field has only a component along the x-direction. Moreover, since the height of the patch is taken to be very small, modes with variation along the x-direction are not excited at the frequencies of interest, so we set $p = 0$. Under these assumptions, the field distribution within the patch is transverse magnetic (TM^x) and can be written as

$$\begin{aligned} E_x(x,\ y,\ z) &= -j\frac{(k_y^2 + k_z^2)}{\omega\mu_0\varepsilon_0\varepsilon_r} A_{mn}\cos(k_y x)\cos(k_z y) \\ H_y(x,\ y,\ z) &= -\frac{k_z}{\mu_0} A_{mn}\cos(k_y y)\sin(k_z z) \\ H_z(x,\ y,\ z) &= \frac{k_y}{\mu_0} A_{mn}\sin(k_y y)\cos(k_z z). \end{aligned} \tag{2}$$

In the previous expressions, ε_0 and μ_0 are the electric permittivity and magnetic permeability of free space, respectively; ε_r is the relative permittivity of the medium underneath the patch. The corresponding resonance frequencies are given by

$$\nu_{mn} = \frac{1}{2\sqrt{\mu\varepsilon}}\sqrt{\left(\frac{m}{W}\right)^2 + \left(\frac{n}{L}\right)^2}. \tag{3}$$

The patch antenna radiates from effect source currents located at the slot openings along the periphery of the patch. Based on the equivalence principle, these effective source currents can be estimated by replacing the electric fields $\mathbf{E}_a$ at the surface of the slots by fictitious magnetic currents related to the surface fields according to

$$\mathbf{M}_s = -2\hat{n} \times \mathbf{E}_a. \tag{4}$$

A variety of formulas exist that correct the effective length of the patch for the effects of fringing fields at the slot openings; such corrections slightly alter the resonance frequencies and characteristics of the modes, as well as the radiated power. We will not consider such corrections here, as our primary goal is to obtain insight rather than produce a complete design tool.

In the following, we will restrict our analysis to the lowest TM^x_{010} mode, for which Eq. (2) reduces to

$$\begin{aligned} E_x(x,\ y,\ z) &= E_0\cos\left(\frac{\pi}{W}y\right) \\ H_z(x,\ y,\ z) &= H_0\sin\left(\frac{\pi}{W}y\right). \end{aligned} \tag{5}$$

This mode is TEM and is similar to the plasmonic patch mode that will be considered below. For such a mode, the transmission line model can be applied to determine the coupling of a magnetic driving field to the resonant fields within the patch, as will be described shortly.

The far-field radiation pattern for the mode specified by Eq. (5) can be calculated using the effective source current density of Eq. (4), yielding[32]

$$\begin{aligned} E_r \sim E_\theta &= 0 \\ E_\varphi &= +j\frac{k_0 hLE_0 e^{-jk_0 r}}{2\pi r}\left\{\sin\theta\frac{\sin X}{X}\frac{\sin Z}{Z}\right\} \\ H_\theta &= E_\varphi/\eta_0, \end{aligned} \tag{6}$$

where

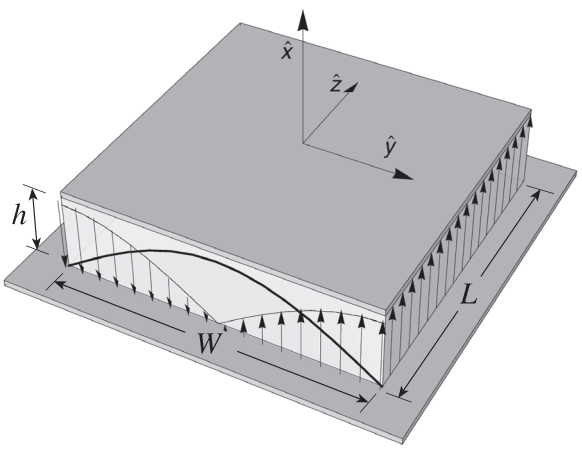

FIG. 1. Diagram of a conventional patch antenna showing the coordinate system. The arrows indicate the strength and direction of the electric field and the thick, solid line indicates the magnitude of the magnetic field of the TM^x_{010} resonant mode.

$$X = \frac{k_0 h}{2}\sin\theta\cos\varphi$$
$$Z = \frac{k_0 L}{2}\cos\theta. \tag{7}$$

Here, θ is taken from the positive z-axis while φ is in the xy plane and taken from the x-axis; η_0 is the impedance of free space. Equation (6) represents the radiation pattern for a single slot; for the two slots, an array factor must be included of the form,[32]

$$(AF)_y = 2\cos\left(\frac{k_0 W}{2}\sin\theta\sin\varphi\right). \tag{8}$$

The above analysis provides a compact summary of the properties of the patch antenna, but does not provide a means to compute the coupling of the antenna to an incident wave. Typically, an antenna feed is considered as part of the system and the antenna gain, directivity and similar parameters are of interest. In the present context, however, we are interested in the scattering properties of the patch, and must apply a model that connects the local fields of the patch to the fields of the incident wave. To fully model the response of the patch, we must also include the effects of radiation resistance. In the absence of radiation resistance, an otherwise lossless patch would produce infinitely large local fields in response to an incident field of any magnitude.

III. TRANSMISSION LINE MODEL OF PATCH

Because the ground plane produces an electromagnetic image of the upper patch, the optical patch antenna is similar to the "cut-wire pair" structure used to produce artificially magnetic metamaterials.[33] The cut-wire pair can be thought of as being excited by the magnetic flux that flows in the gap between the separated metallic wires or plates. As described above, the mode propagating within the plate is to a good approximation TEM, so that a transmission line analysis can be properly formulated and the details of the system can be replaced by the equivalent circuit shown in Fig. 2. The quantities R'_s, C'_S, and L'_S are the series resistance per unit length, shunt capacitance per unit length, and series inductance per unit length. The effective transmission line terminates at either edge of the patch in an effective lumped radiation resistance, R_r. The explicit expressions for the resistances will be derived in Secs. V and VI. In particular, we will show that R_r can be obtained from the scattering characteristics of the patch antenna, while R'_s will require the calculation of the propagation losses of the gap-plasmon mode associated to the optical patch antenna.

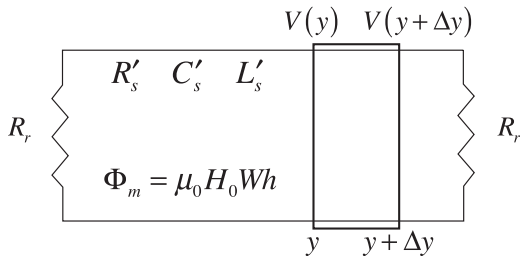

FIG. 2. Equivalent circuit of the magnetically driven patch antenna.

In order calculate, the induced current and voltage on the patch as a function of the incident field, we begin by assuming the incident plane wave is incident normally onto the patch (i.e., along the negative x-direction), and is polarized such that the magnetic field lies along the z-direction. A transmission line circuit similar to that shown in Fig. 2 has been used in the analysis of plasmonic wire pairs, where the two lines correspond to the patch and ground plane. To find the induced current and voltage along the patch as a function of the driving flux from the incident field, we adopt the technique used by Lagarkov and Sarychev.[34] The electromagnetic force induced around a loop enclosing magnetic flux can be found by integrating the Maxwell curl equation,

$$\nabla\times\mathbf{E} = -\frac{\partial\mathbf{B}}{\partial t}. \tag{9}$$

Integrating Eq. (9) around a differential loop of area $h\Delta y$, we obtain

$$V(y+\Delta y) - V(y) = -I(y)Z - j\omega\mu_0 2H_0 h\Delta y. \tag{10}$$

Performing a Taylor expansion on the voltage, we have

$$\frac{\partial V(y)}{\partial y} = -I(y)Z' - j\omega\mu_0 2H_0 h, \tag{11}$$

where $Z' = R'_S + j\omega L'_S$. The factor of two on the right hand side of Eq. (11) accounts for the reflected field, which doubles the incident magnetic field. In the usual manner, a second equation can be found by considering the displacement current shunted across the line

$$\frac{\partial I(y)}{\partial y} = j\omega C'_S V(y). \tag{12}$$

From these two equations, we obtain an expression for the current as a function of position along the transmission line, or

$$\frac{\partial^2 I(y)}{\partial y^2} = g^2 I(y) + F, \tag{13}$$

where

$$g^2 = -j\omega C'_S Z'$$
$$F = 2\omega^2 C'_S \mu_0 h H_0. \tag{14}$$

Equation (13) can be solved to obtain the general solution

$$I(y) = \frac{F}{g^2} + A\cos(gy) + B\sin(gy)$$
$$V(y) = \frac{Ag\sin(gy)}{j\omega C'_S} - \frac{Bg\cos(gy)}{j\omega C'_S}, \tag{15}$$

where A and B are arbitrary coefficients to be determined by the boundary conditions. Based on the mirror symmetry of the configuration, we assume the symmetric solution and set $B = 0$ to arrive at the following condition:

$$\frac{V(W/2)}{I(W/2)} = \frac{\dfrac{Ag\sin\left(\frac{gW}{2}\right)}{j\omega C'_S}}{\dfrac{F}{g^2} + A\cos\left(\dfrac{gW}{2}\right)} = R_r, \tag{16}$$

from which we find

$$A = \frac{\dfrac{j\omega C'_S R_r F}{g^2}}{g\sin\left(\dfrac{gW}{2}\right) - j\omega C'_S R_r \cos\left(\dfrac{gW}{2}\right)}. \tag{17}$$

Equations (15) and (17) then provide the complete solution for the induced current and voltage on the patch as a function of the incident field.

IV. FIELD ENHANCEMENT OF THE RESONANT PATCH

The peak voltages on the patch for the TM^x_{010} mode occur at the slots located at $y = \pm W/2$, as depicted in Fig. 1. Knowledge of the voltage at these points combined with the mode specification of Eq. (5) then allows determination of both the fields everywhere inside the patch as well as the power radiated. From Eqs. (15) and (17), we find the voltage at the slot located at $y = +W/2$ to be

$$V\left(\frac{W}{2}\right) = \frac{\dfrac{R_r F}{g}}{g\sin\left(\dfrac{gW}{2}\right) - j\omega C'_S R_r \cos\left(\dfrac{gW}{2}\right)}\sin\left(\frac{gW}{2}\right). \tag{18}$$

Writing Eq. (18) in terms of the field, and normalizing with respect to the incident field, we obtain

$$\frac{E\left(\frac{W}{2}\right)}{E_0} = \frac{\dfrac{2R_r\omega^2 C'_S\mu_0}{g\eta_0}}{g\sin\left(\dfrac{gW}{2}\right) - j\omega C'_S R_r\cos\left(\dfrac{gW}{2}\right)}\sin\left(\frac{gW}{2}\right). \tag{19}$$

The per unit length shunt capacitance, assuming no dielectric spacer, can be approximated as that of a parallel plate capacitor, or

$$C'_S = \varepsilon_0\frac{W}{h}. \tag{20}$$

For the plasmonic patch to be considered below, Eq. (20) should be multiplied by a factor of $\beta h + e^{-\beta h}$ (where β is the transmission line propagation constant) to account for both intra-plate and cross-plate capacitances.[35] However, in the limit of small gaps, $\beta h \ll 1$ so that $(\beta h + e^{-\beta h}) \sim 1$. Thus, Eq. (20) remains unchanged for the configurations considered here.

The expression for the per unit length inductance for either the standard patch or the plasmonic patch is more complicated, since either skin depth effects at lower frequencies[32] or kinetic inductance at optical wavelengths[31] play a significant role. We are able to bypass the explicit consideration of the inductance, L'_S, however, which enters the equations everywhere as a product with the per unit length capacitance, $L'_S C'_S$. Since the transmission line propagation constant has the form $\beta^2 = \omega^2 L'_S C'_S$, we can make use of the dispersion relation to determine β directly. With this subsequent substitution in mind, we write

$$\begin{aligned} g^2 &= -j\omega C'_S Z' = -j\omega C'_S(R'_S + j\omega L'_S) \\ &= -j\omega C'_S R'_S + \omega^2 L'_S C'_S \\ &= \beta^2 - j\omega C'_S R'_S, \end{aligned} \tag{21}$$

where

$$\beta = \frac{2\pi n_g}{\lambda_0}. \tag{22}$$

In Eq. (22), n_g is the effective index associated with the waveguide mode. Inserting the expression in Eq. (20) for the capacitance into Eq. (19), we obtain

$$f = \frac{2\dfrac{k_0}{g}\dfrac{R_r}{\eta_0}\dfrac{W}{h}}{\dfrac{g}{k_0}\sin\left(\dfrac{gW}{2}\right) - j\left(\dfrac{W}{h}\right)\dfrac{R_r}{\eta_0}\cos\left(\dfrac{gW}{2}\right)}\sin\left(\frac{gW}{2}\right) \tag{23}$$

and

$$g^2 = \beta^2 - jk_0\frac{W}{h}\frac{R'_S}{\eta_0}, \tag{24}$$

where $f = E(W/2)/E_0$ is the field enhancement.

There are two interesting limits to observe from the above equations. In the absence of radiative losses, $R_r \to \infty$, and Eq. (23) reduces to

$$f_{R_r\to\infty} = -2j\frac{k_0}{g}\tan\left(\frac{gW}{2}\right). \tag{25}$$

We are interested in the behavior of the patch at resonance at which, in the absence of losses, the wavelength in the guide is twice the width of the guide, or

$$\lambda_r = 2W. \tag{26}$$

In the absence of losses, this condition equates to

$$g\frac{W}{2} = \beta\frac{W}{2} = \frac{\pi}{2}. \tag{27}$$

If the resistive losses are taken as very small rather than zero, the resonance condition is not altered much, but we can approximate

$$g \simeq \beta - j\frac{k_0}{\beta}\frac{W}{2h}\frac{R'_S}{\eta_0}. \tag{28}$$

Inserting Eq. (28) into Eq. (25) and using the resonance condition of Eq. (27), we obtain an approximate expression for the local field enhancement in the absence of radiative losses of

$$f_{R_r\to\infty} = 8\left(\frac{h}{W}\right)\left(\frac{\eta_0}{WR'_S}\right). \tag{29}$$

Thus, we see that in the absence of either resistive or radiative losses, the local field enhancement diverges at resonance as expected for a resonant circuit. The inclusion of resistive losses makes the resonance fields finite and also introduces a slight shift to the resonance frequency that we do not consider further.

If the radiation resistance is finite, then we can safely take the limit of zero absorptive losses ($R'_S \to \infty$) in Eq. (23), setting the cosine term in the denominator to zero, such that

$$f_{R'_S\to\infty} = \frac{2}{n_g^2}\frac{R_r}{\eta_0}\frac{W}{h}. \tag{30}$$

Equation (30) is particularly useful for comparison with numerical simulations, since resistive losses can be switched off and radiation damping made the only loss mechanism. Note that as the radiation resistance increases, the local field enhancement increases without bound, as would be expected for a lossless resonator.

V. CALCULATION OF RADIATIVE LOSSES

It remains now to calculate values for the various loss factors that will complete our parameterization of the optical patch. To calculate the radiation resistance, we start by considering the field distribution for the particular polarization under consideration. For this polarization, only the H_θ and E_φ components exist, so that from Eq. (6) we can write

$$\begin{aligned} E_\varphi &= +j\frac{k_0 hLE_0 e^{-jk_0 r}}{2\pi r} f(\theta,\,\varphi) \\ H_\theta &= E_\varphi/\eta_0, \end{aligned} \tag{31}$$

where $f(\theta,\,\varphi)$ is a dimensionless function of the angular coordinates. Recall that the field distribution in Eq. (6) arises from an effective magnetic current assumed to be generated at the slot of the patch. The total radiated power can be computed from Eq. (31) as[32]

$$\begin{aligned} P_{rad} &= \frac{1}{2\eta_0}\left(\frac{L}{\lambda_0}\right)^2 (hE_0)^2 \int_0^\pi\int_0^\pi f^2(\theta,\,\varphi)\sin\theta\, d\theta\, d\varphi \\ &= \frac{V^2}{2\eta_0}\left(\frac{L}{\lambda_0}\right)^2 \int_0^\pi\int_0^\pi f^2(\theta,\,\varphi)\sin\theta\, d\theta\, d\varphi. \end{aligned} \tag{32}$$

We have introduced the driving voltage $V = hE_0$, which arises from the equivalence principle. Assuming the gap length is very small, we write

$$f(\theta,\,\varphi) = 2\cos\left(\frac{k_0 W}{2}\sin\theta\sin\varphi\right)\sin\theta\frac{\sin\left(\frac{k_0 L}{2}\cos\theta\right)}{\frac{k_0 L}{2}\cos\theta}, \tag{33}$$

so that

$$P_{rad} = \frac{V^2}{R_r} = \frac{2V^2}{\eta_0}\left(\frac{I_1}{\pi^2}\right), \tag{34}$$

where

$$\begin{aligned} R_r &= \frac{\pi^2\eta_0}{2I_1} \\ I_1 &= \int_0^\pi\int_0^\pi \cos^2\left(\frac{k_0 W}{2}\sin\theta\sin\varphi\right)\sin^3\theta\frac{\sin^2\left(\frac{k_0 L}{2}\cos\theta\right)}{\cos^2\theta}d\theta d\varphi. \end{aligned} \tag{35}$$

Note that due to the large effective index, the overall size of an optical patch can be much smaller than the wavelength. Thus, the integral I_1 can be substantially smaller than for microwave patch antennas, with the corresponding radiation resistance values much higher ($\sim$0.8–4.5 kΩ). For reference later below, the computed radiation resistance for a $W = 80$ nm silver patch antenna is about 1.5 kΩ.

VI. PLASMONIC EFFECTS AND RESISTIVE LOSSES

Since our goal is to understand the enhancement associated with nanoantennas at optical wavelengths, we must consider in more detail the effect of the metal. The radiation damping term would not be expected to change significantly, at least given our assumptions above; however, losses must be calculated assuming a more accurate field distribution within the metal. In this section we review the details of the gap plasmon mode and then find an approximate expression for the transmission line effective resistance per unit length.

At optical wavelengths, the metal cannot be assumed perfect, and a significant amount of field will extend into the metal regions. The nature of the cavity solutions, obtained for the case of a perfect metal by assuming the guided mode solutions in Eq. (2), will change to reflect the modified boundary condition on top and bottom of the cavity. Here we focus again on the lowest order mode that can propagate in the gap.

Using the same coordinate system as before, we can write the field solutions in the gap between two infinite metal regions, assuming continuity of the tangential components of the electric and magnetic fields across the interfaces. We first assume the magnetic field solution

$$\mathbf{H} = \begin{cases} H_z^I \hat{z} e^{\kappa x} e^{-jk_y y} & x < -h/2 \\ \hat{z} H_z^{II}\cos(k_x x) e^{-jk_y y} & -h/2 < x < h/2\,, \\ H_z^{III}\hat{z} e^{-\kappa x} e^{-jk_y y} & h/2 < x \end{cases} \tag{36}$$

where $k_x = \sqrt{k_y^2 - k_0^2}$ and $\kappa = \sqrt{k_y^2 - \varepsilon'(\omega)k_0^2}$. This is a symmetric mode that will turn out to be analogous to the TM_{010}^x mode considered above, allowing us to make use of all formulas previously derived. We can relate the electric field to the magnetic field components in Eq. (36) using

$$\nabla\times\mathbf{H} = j\omega\varepsilon(\omega)\mathbf{E}, \tag{37}$$

from which we find

$$E_x = \frac{1}{j\omega\varepsilon(\omega)}\left(\frac{\partial H_z}{\partial y}\right)$$
$$E_y = -\frac{1}{j\omega\varepsilon(\omega)}\left(\frac{\partial H_z}{\partial x}\right). \tag{38}$$

Here, $\varepsilon(\omega) = \varepsilon'(\omega) + j\varepsilon''(\omega)$ is the dielectric function of metal. The electric field in the three regions can then be written as

$$\mathbf{E} = \begin{cases} H_z^I\left(-\frac{k_y}{\omega\varepsilon(\omega)}\hat{x}e^{\kappa x} - \frac{\kappa}{j\omega\varepsilon(\omega)}\hat{y}e^{\kappa x}\right) & x < -h/2 \\ H_z^{II}\left(-\frac{k_y}{\omega}\hat{x}\cos(k_x x) + \frac{k_x}{\omega}\sin(k_x x)\hat{y}\right) & -h/2 < x < h/2. \\ H_z^{III}\left(-\frac{k_y}{\omega\varepsilon(\omega)}\hat{x}e^{-\kappa x} + \frac{\kappa}{j\omega\varepsilon(\omega)}\hat{y}e^{-\kappa x}\right) & h/2 < x \end{cases} \tag{39}$$

In writing Eq. (39), we omitted the common factor $\exp(-jk_y y)$ in all of the expressions. Setting the tangential components of the magnetic field equal at the two interfaces, we obtain from Eq. (36)

$$H_z^{II}\cos\left(\frac{k_x h}{2}\right) = H_z^I e^{-\frac{k_x h}{2}}. \tag{40}$$

Setting the tangential components of the electric field equal at the two interfaces, we obtain from Eq. (39)

$$-H_z^{II}\sin\left(\frac{k_x h}{2}\right) = -H_z^I\frac{\kappa}{jk_x\varepsilon(\omega)}e^{-\frac{k_x h}{2}}. \tag{41}$$

Dividing Eq. (41) by Eq. (40), we obtain the dispersion relation for the gap plasmon

$$\tan\left(\frac{k_x h}{2}\right) = -j\frac{\kappa}{k_x\varepsilon(\omega)}. \tag{42}$$

In the absence of loss, $\varepsilon(\omega) = \varepsilon'(\omega)$, Eq. (42) has solutions only for imaginary k_x, so we arrive at the final form of the dispersion relation

$$k_x\tanh\left(\frac{k_x h}{2}\right) + \frac{\kappa}{\varepsilon'(\omega)} = 0. \tag{43}$$

Using Eq. (43), we can determine the propagation constant k_y for the wave propagating within the gap. As an example, we will consider silver nanocubes interacting with a silver film. Using published data[36] for the real part of the dielectric function of silver in Eq. (43), we solve for k_y and plot the ratio $n_g = k_y/k_0$ in Fig. 3.

Note from the solution of Eq. (36) that, in general, the gap plasmon has fields that vary along both the x and y directions and, in particular, electric fields that vary in both the x and y directions. However, from Eq. (39) we see that the ratio of the y to the x component of the electric field is

$$\frac{|E_y|}{|E_x|} = \frac{k_y}{k_x}\tan(k_x h). \tag{44}$$

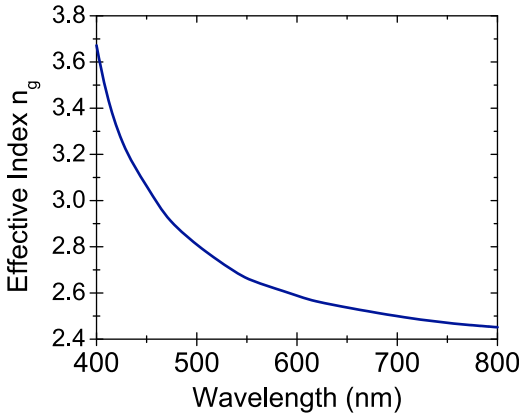

FIG. 3. Effective guide index for the gap-plasmon mode associated to the metal-air-metal waveguide. The metal regions extend infinitely and are separated by a distance of 10 nm. Metal is assumed to be silver.

For large effective mode index $k_x \sim k_y$, we see from Eq. (44) that the y-component of the electric field can be extremely small due to the small size of the gap relative to the wavelength. The transmission line framework outlined above, then, remains applicable even to the optical patch.

To determine the losses in the above transmission line model, the resistance per unit length must be calculated. In the presence of losses, a voltage or current wave traveling along a transmission line has the form $\exp(\gamma y)$, where $\gamma = jg = -\alpha - j\beta$. A straightforward means of determining the transmission line parameters would be to solve the dispersion equation, Eq. (43), for the complex k_y and compare the real and imaginary parts. In the spirit of obtaining analytic expressions, however, we attempt here a perturbative solution assuming that the resistance per unit length is very small. In this limit, the transmission line voltage decays with length at a rate of

$$\alpha \simeq \frac{R_S'}{2}\sqrt{\frac{C_S'}{L_S'}} = \frac{R_S' C_S'}{2}\sqrt{\frac{1}{L_S' C_S'}}$$
$$= \frac{R_S'}{2\eta_0}\frac{W}{h n_g}. \tag{45}$$

We have made use of the expression for the capacitance to obtain the final form in Eq. (45).

If one now allows for a complex dielectric function ($\varepsilon \to \varepsilon' - j\varepsilon''$), the wavenumber determined from Eq. (42) will be complex; that is,

$$k_y \to k_y + j\tilde{k}_y, \tag{46}$$

where we expect the imaginary part of the wave number to be proportional to the imaginary part of the dielectric function. Substituting this form of the y-component of the propagation vector into Eq. (43) and expanding all terms up to the first order, we obtain

$$\tilde{k}_y \simeq \frac{\kappa\varepsilon''}{\left(\left(\tanh\left(\frac{k_x h}{2}\right) + \frac{k_x h}{2}\right)\frac{n_g\varepsilon'^2}{\sqrt{n_g^2 - 1}} - \frac{n_g\varepsilon'}{\sqrt{n_g^2 - \varepsilon'}}\right)}. \tag{47}$$

In calculating Eq. (47) we neglected terms containing products of the from: $\tilde{k}_y\varepsilon''$, ε''^2, etc. It is clear from Eq. (47) that resistive losses increase with ε'' as well as with κ. Here, κ^{-1} plays a role akin to the skin depth of a conventional conductor, indicating the extent that the fields penetrate into the metal regions. Comparing Eq. (47) with Eq. (45), we find

$$R_S' = \eta_0 \frac{2hn_g}{W} \frac{\kappa\varepsilon''}{\left(\left(\tanh\left(\frac{k_x h}{2}\right) + \frac{k_x h}{2}\right)\frac{n_g\varepsilon'^2}{\sqrt{n_g^2-1}} - \frac{n_g\varepsilon'}{\sqrt{n_g^2-\varepsilon'}}\right)}. \tag{48}$$

Recalling that $k_x = k_0\sqrt{n_g^2-1}$ and $\kappa = k_0\sqrt{n_g^2-\varepsilon'(\omega)}$, we find an approximate expression for the resistance per unit length based on the known geometry and material parameters of the patch. We have confirmed the validity of Eq. (48) by computing the complex mode propagation constant numerically; extremely good agreement is found between the two methods, indicating the assumptions made in arriving at Eq. (48) are appropriate. Note that Eqs. (47) and (48) are in general valid for any gap size, provided losses are small. In the limit of small gaps, such that $\tanh(x) \simeq x$, alternative approximate formulas can be easily found.[37]

To get an idea of the order of magnitude of the per unit length resistance, we solve Eq. (48) assuming the dielectric function data from Johnson and Christy[36] and a cube of dimension $W = 80$ nm spaced a distance $h = 10$ nm above a film. The resulting curve is shown in Fig. 4. For this cube, it will be shown in Sec. VII that the resonance wavelength occurs around $\lambda = 530$ nm where there is a significant drop in the loss.

VII. SPECIFIC EXAMPLES

Having fixed the nanocube side length W, we solve self-consistently the equation,

$$\lambda_r = 2Wn_g(\lambda_r), \tag{49}$$

to determine the resonance wavelength, λ_r. Alternatively, we can infer the effective mode index by observing the position of the resonance in a full wave simulation. However, because

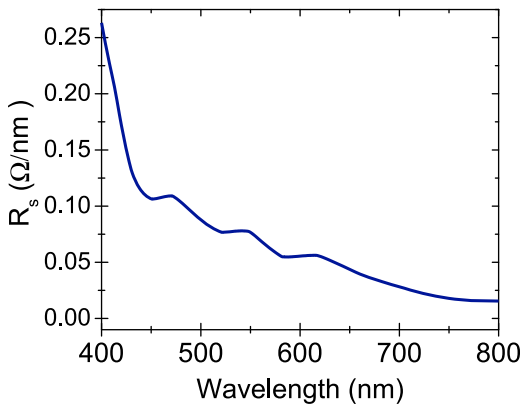

FIG. 4. Resistance per unit length [Ω/nm] of the transmission line mode as a function of wavelength, as calculated using Eq. (48).

of the fringing effects, the nanocube tends to be electrically larger than its physical dimension. The fringing fields indicate that the boundary conditions at the slot surfaces are not strictly magnetic, so that an additive correction,[38] Δ that alters the resonance condition is required. Equation (49) then can be modified as

$$\lambda_r = 2W_{eff}n_g(\lambda_r) = 2(W+2\Delta)n_g(\lambda_r). \tag{50}$$

Based on full wave simulations, for a cube size of $W = 80$ nm with a gap of $h = 10$ nm, we find $\Delta = 9.2$ nm and the resonance wavelength for the silver cube to be near $\lambda_r = 530$ nm. In general, to find the appropriate resonance conditions we must appeal to full-wave simulations.

At this point, some considerations on the effect of the plasmonic nature of the patch on the coupling with the incident fields are required. As we have shown above, a significant amount of field extends into the metal regions. In particular, this will alter the amount of magnetic flux flowing through the patch. The integration of Maxwell's curl equation (9) should be then extended to a larger area to properly include that portion of the magnetic field penetrating the metal. The effect can be captured by considering the loop area to be $(h+2\delta)\Delta y$, where $\delta = 1/\sqrt{\beta^2 - \varepsilon k_0^2}$ indicates the fields penetration depth. The effect of increasing the magnetic flux directly impacts the maximum field enhancement by a factor of $(1+2\delta/h)$. Equation (23) then becomes

$$f = \frac{2\frac{k_0}{g}\frac{R_r}{\eta_0}\frac{W}{h}\left(1+2\frac{\delta}{h}\right)}{\frac{g}{k_0}\sin\left(\frac{gW}{2}\right) - j\left(\frac{W}{h}\right)\frac{R_r}{\eta_0}\cos\left(\frac{gW}{2}\right)}\sin\left(\frac{gW}{2}\right). \tag{51}$$

At visible frequencies, this modification introduces an important correction that enhances the electric field enhancement by an additional factor of ~10–15.

Having found the series resistance per unit length and the radiation resistance in the previous sections, we can now compute the electric field enhancements within the patch. In the absence of resistive losses, we find the enhancement curve shown in Fig. 5. At resonance, the local field is roughly 55 times that of the incident field at the slot, falling off towards the interior of the patch. The peak field coincides exactly with Eq. (30).

When the resistive losses indicated in Fig. 4 are included, the peak field enhancement is reduced and the curve broadens somewhat. We see the peak field enhancement is reduced to about 40.

VIII. VALIDATION

To demonstrate the validity of our model we perform in this section a series of comparisons with full-wave simulations. In Ref. 27 an optical analog of the microwave patch antenna was fabricated using colloidal silver nanocubes. In our theory, we implicitly assumed that the thickness of the patch does play a negligible role in determining the field enhancements. This is particularly true considering the simplicity of the approach adopted. For this reason and because

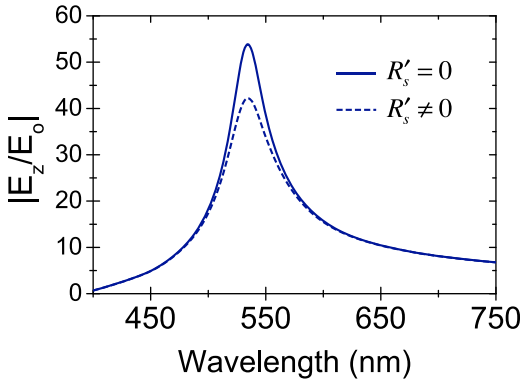

FIG. 5. Local electric field enhancement as a function of wavelength for a $W = 80$ nm cube spaced 10 nm from film. Only radiative losses are included, not resistive (solid line). Both radiative and resistive losses are included (dotted line).

of the actual implementation of the system, we will consider in this paragraph patches constituted by cubic nanoparticles. Numerical simulations are carried out using a commercial electromagnetic mode solver based on the finite-element method, COMSOL Multiphysics. In the simulations, an incident wave is directed onto a single silver nanocube positioned a distance h above a 50 nm thick silver film. The wave is incident parallel to the surface normal of the film. To avoid numerical artifacts, we round the edges of the nanocube to a radius of 7 nm. The cross-section of the simulated geometry is shown in the inset of Fig. 6. The incident field is specified analytically for the bare film geometry, and the resulting scattered field due to the presence of the nanocube can then be solved for using the scattered field formulation.[26] As was done for the analytical studies above, Johnson and Christy data[36] are used to define the optical properties of silver in the full-wave simulation. Both the volumes above and underneath the silver film are defined to be vacuum ($n = 1$). Figure 6 shows a comparison of full-wave simulations to plasmonic patch theory for several nanocube sizes and separation distances.

As mentioned in Sec. VII, for the resonances predicted by the theory to match simulations a correction must be applied to account for the reflection phase shift at the slots. The effective dimension of the nanocube is then $W_{eff} = L_{eff} = W + 2\Delta$. To obtain Δ, we must perform a full-wave simulation for each gap size, h. In Fig. 6, the correction factors are found as follows: for $h = 5$ nm, $\Delta = 1.2$ nm; for $h = 10$ nm, $\Delta = 9.2$ nm; and for $h = 15$ nm, $\Delta = 15.6$ nm. Once Δ is obtained using one simulation for a given gap size, the theory then accurately predicts the resonance positions for other nanocube sizes, as shown in Fig. 6. For each gap size, Δ was obtained using the 80 nm nanocube, yet the theory still accurately predicts the resonance positions for both the 70 nm and 90 nm nanocube sizes.

As can be seen from Fig. 6, the theory predicts very well both the field enhancement and spectral characteristics of the fundamental mode resonance. The agreement is striking considering the simplicity of our model. However, as the gap size is reduced, the agreement of theory with full-wave simulations worsens. The same disagreement persists also in the absence of resistive losses, as shown in Fig. 7, where field

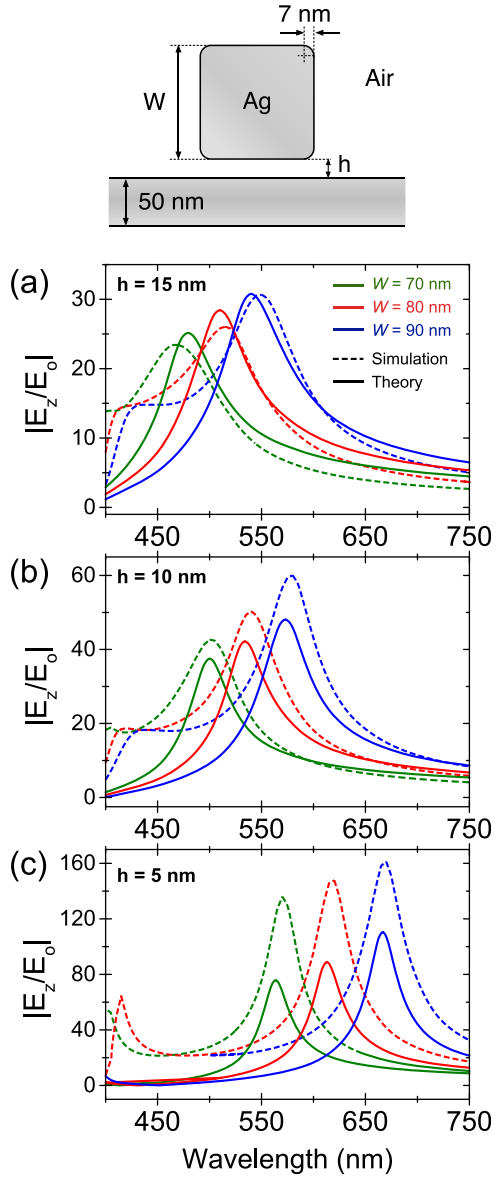

FIG. 6. Comparison of full-wave simulations (dashed lines) to patch antenna theory (solid lines) for several nanocube sizes: $W = 70$ nm (green), $W = 80$ nm (red), and $W = 90$ nm (blue). Here, the ordinates represent the modulus of the enhancement factor for the electric field (vertical component) in the gap. The values are taken at the edge of the nanocube ($y = W/2$) where the field is maximized. The nanocubes were positioned a distance, h, above the ground plane metal film: (a) $h = 15$ nm, (b) $h = 10$ nm, (c) $h = 5$ nm. On the top, a schematic of the simulated geometry.

enhancements were calculated neglecting absorption losses in the metal ($\varepsilon(\omega) = \varepsilon'(\omega)$), for a 80 nm nanocube spaced only 5 nm from the film. These results are not surprising, considering the details, for example, of the rounded edges used in the simulations that are not captured by our analytic expressions. In fact, the local field distribution at the edges can be relatively complex and no doubt has a significant impact on the field enhancement. By the time the nanocube is only 5 nm from the film, the edge rounding is no longer negligible in comparison with the critical dimensions. Sharpening the nanocube edges however, only partially accounts for the difference. Another cause for the disagreement can be found in the coupling of the nanocubes with the surface plasmon propagating along the film surface, which

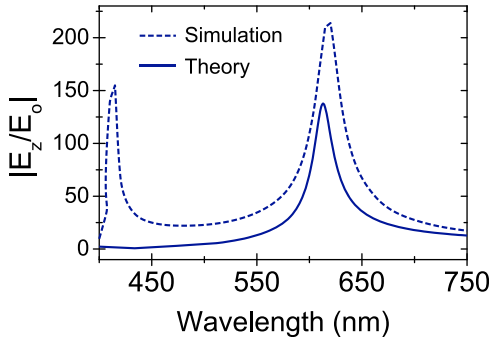

FIG. 7. Comparison of theory (solid line) and full-wave simulations (dotted line). Local electric field enhancement as a function of wavelength for a $W = 80$ nm cube spaced 5 nm from film. Only radiative losses are included.

could introduce an important modification of the radiation resistance, and it is completely neglected by the theory.

IX. CONCLUSION

We have introduced a simple, yet comprehensive model for describing patch antennas at optical frequencies. The introduction of an equivalent circuit was indispensable for two reasons. On the one hand, it enables the description of interaction of the system with an incident field in a very simple and enlightening way; on the other hand, it allows an independent description for radiative and absorption properties. The radiative characteristics are described through the well-known microstrip patch antenna theory, which we have shown retains its applicability even when the patch is substituted with a cube. That the patch theory remains valid stems from the fact that at optical frequencies, a nanocube is much smaller than its resonance wavelength. The impact of the cube on the radiation properties of the slots is then negligible and the effective magnetic currents radiate as if in free-space; that is, the equivalence principle used for planar patches is unchanged.

While the majority of nanoplasmonic systems require full-wave simulations to accurately assess their optical properties, the film-coupled planar nanoparticle geometry is somewhat more amenable to analytical approaches since it conforms mostly to the planar patch geometry. Departures from the traditional patch theory are mostly contained within the dispersion relation for the gap plasmon mode, which we have used to complete the analysis. The effective waveguide index that results from the gap dispersion relation can be used, for example, to bypass what would be a much more complicated analytical calculation of the per unit length inductance. Likewise, we find that the resistive losses in the plasmonic patch antenna are small enough that a perturbative approach can be applied to the dispersion relation, revealing that the resistance per unit length is directly proportional to the gap plasmon mode absorption.

The plasmonic nature of the optical patch has a strong impact on the coupling of the patch to the incident wave. Our model shows that the fundamental mode underneath the nanocube is exclusively excited by the incident magnetic field. At optical wavelengths, where the metal response is more dielectric-like than conductor-like, the coupling with the incident wave is increased by roughly a factor of 10 compared with the case of a perfectly conducting patch. This increase is due to the greater penetration of the magnetic field into the metal, which results in a larger flux area as compared with that proscribed by the gap.

We believe the model as presented not only provides a useful glimpse into the underlying physics of the plasmonic patch antenna system—offering useful insights for potential applications—but also provides accurate predictions of the patch behavior. These characteristics make the optical patch system a valuable tool that may potentially be applied to further analytical calculations of other phenomena of interest, including controlled reflectance and enhanced fluorescence.

ACKNOWLEDGMENTS

This work was supported by the Air Force Office of Scientific Research (AFOSR), (Grant No. FA9550-09-1-0562).

[1]M. Moskovits, "Surface-enhanced spectroscopies," Rev. Mod. Phys. **57**, 783 (1985).
[2]M. Neviere and R. Reinisch, "Electromagnetic study of the surface-plasmon-resonance contribution to surface-enhanced Raman scattering," Phys. Rev. B **26**, 5403 (1982).
[3]J. R. Lakowicz, "Radiative decay engineering 5: Metal-enhanced fluorescence and plasmon emission," Anal. Biochem. **337**, 171–194 (2005).
[4]M. Kauranen and A. V. Zayats, "Nonlinear plasmonics," Nat. Photonics **6**, 737–748 (2012).
[5]J. J. Mock, R. T. Hill, Y.-J. Tsai, A. Chilkoti, and D. R. Smith, "Probing dynamically tunable localized surface plasmon resonances of film-coupled nanoparticles by evanescent wave excitation," Nano Lett. **12**, 1757 (2012).
[6]D. J. Bergman and M. I. Stockman, "Surface plasmon amplification by stimulated emission of radiation: Quantum generation of coherent surface plasmons in nanosystems," Phys. Rev. Lett. **90**, 027402 (2003).
[7]Y.-J. Lu *et al.*, "Plasmonic nanolaser using epitaxially grown silver film," Science **337**, 450 (2012).
[8]E. Plum, V. A. Fedotov, P. Kuo, D. P. Tsai, and N. I. Zheludev, "Towards the lasing spaser: Controlling metamaterial optical response with semiconductor quantum dots," Opt. Express **17**, 8548 (2009).
[9]R. F. Oulton *et al.*, "Plasmon lasers at deep subwavelength scale," Nature **461**, 629 (2009).
[10]M. A. Noginov *et al.*, "Demonstration of a spaser-based nanolaser," Nature **460**, 1110 (2009).
[11]J. Kottmann, O. J. F. Martin, D. R. Smith, and S. Schultz, "Dramatic localized electromagnetic enhancement in plasmon resonant nanowires," Chem. Phys. Lett. **341**, 1 (2001).
[12]F. Garcia-Vidal and J. B. Pendry, "Collective theory for surface-enhanced Raman scattering," Phys. Rev. Lett. **77**, 1163 (1996).
[13]A. Aubry, D. Y. Lei, A. I. Fernandez-Dominguez, Y. Sonnefraud, S. A. Maier, and J. B. Pendry, "Plasmonic light-harvesting devices over the whole visible spectrum," Nano Lett. **10**, 2574 (2010).
[14]P. K. Aravind, R. W. Rendell, and H. Metiu, "A new geometry for field enhancement in surface-enhanced spectroscopy," Chem. Phys. Lett. **85**, 396 (1982).
[15]J. K. Daniels and G. Chumanov, "Nanoparticle-mirror sandwich substrates for surface-enhanced Raman scattering," J. Phys. Chem. B **109**, 17936 (2005).
[16]D. J. Anderson and M. Moskovits, "A SERS-active system based on silver nanoparticles tethered to a deposited silver film," J. Phys. Chem. B **110**, 13722 (2006).
[17]J. D. Driskell, R. J. Lipert, and M. D. Porter, "Labeled gold nanoparticles immobilized at smooth metallic substrates: Systematic investigation of surface plasmon resonance and surface-enhanced Raman scattering," J. Phys. Chem. B **110**, 17444 (2006).
[18]S. Mubeen *et al.*, "Plasmonic properties of gold nanoparticles separated from a gold mirror by an ultrathin oxide," Nano Lett. **12**, 2088 (2012).
[19]J. J. Mock, R. T. Hill, A. Degiron, S. Zauscher, A. Chilkoti, and D. R. Smith, "Distance-dependent plasmon resonant coupling between a gold nanoparticle and gold film," Nano Lett. **8**, 2245–2252 (2008).

[20]W. Rechberger *et al*., "Optical properties of two interacting gold nanoparticles," Opt. Commun. **220**, 137 (2003).
[21]T. Atay, J. H. Song, and A. V. Nurmikko, "Strongly interacting plasmon nanoparticle pairs: From dipole-dipole interaction to conductively coupled regime," Nano Lett. **4**, 1627 (2004).
[22]P. Nordlander, C. Oubre, E. Prodan, K. Li, and M. I. Stockman, "Plasmon hybridization in nanoparticle dimers," Nano Lett. **4**, 899 (2004).
[23]I. Romero, J. Aizpurua, G. W. Bryant, and F. J. García de Abajo, "Plasmons in nearly touching metallic nanoparticles: Singular response in the limit of touching dimers," Opt. Express **14**, 9988 (2006).
[24]R. T. Hill, J. J. Mock, Y. A. Urzhumov, D. S. Sebba, S. J. Oldenburg, S.-Y. Chen, A. A. Lazarides, A. Chilkoti, and D. R. Smith, "Leveraging nanoscale plasmonic modes to achieve reproducible enhancement of light," Nano Lett. **10**, 4150–4154 (2010).
[25]A. Tittl, P. Mai, R. Taubert, D. Dregely, N. Liu, and H. Giessen, "Palladium-based plasmonic perfect absorber in the visible wavelength range and its application to hydrogen sensing," Nano Lett. **11**, 4366 (2011).
[26]C. Ciracì, R. T. Hill, J. J. Mock, Y. Urzhumov, A. I. Fernández-Domínguez, S. A. Maier, J. B. Pendry, A. Chilkoti, and D. R. Smith, "Probing the ultimate limits of plasmonic enhancement," Science **337**, 1072–1074 (2012).
[27]A. Moreau, C. Ciracì, J. J. Mock, R. T. Hill, Q. Wang, B. Wiley, A. Chilkoti, and D. R. Smith, "Controlled-reflectance surfaces with film-coupled colloidal nanoantennas," Nature **492**, 86 (2012).
[28]R. Esteban, T. V. Teperik, and J. J. Greffet, "Optical patch antennas for single photon emission using surface plasmon resonances," Phys. Rev. Lett. **104**, 026802 (2010).
[29]C. Belacel, B. Habert, F. Bigourdan, F. Marquier, J. P. Hugonin, S. M. de Vasconcellos, X. Lafosse, L. Coolen, C. Schwob, C. Javaux, B. Dubertret, J. J. Greffet, P. Senellart, and A. Maitre, "Controlling spontaneous emission with plasmonic optical patch antennas," Nano Lett. **13**, 1516 (2013).
[30]J. A. Dionne, L. A. Sweatlock, H. A. Atwater, and A. Polman, "Plasmon slot waveguides: Towards chip-scale propagation with subwavelength-scale localization," Phys. Rev. B **73**, 035407 (2006).
[31]J. Zhou, T. H. Koschny, M. Kafesaki, E. N. Economou, J. B. Pendry, and C. M. Soukoulis, "Saturation of the magnetic response of split-ring resonators at optical frequencies," Phys. Rev. Lett. **95**, 223902 (2005).
[32]C. A. Balanis, *Antenna Theory: Analysis and Design*, 3rd ed. (John Wiley & Sons, 2005), Chaps. 6 and 14.
[33]V. M. Shalaev, W. Cai, U. K. Chettiar, H.-K. Yuan, A. K. Sarychev, V. P. Drachev, and A. V. Kildishev, "Negative index of refraction in optical metamaterials," Opt. Lett. **30**, 3356 (2005).
[34]A. Lagarkov and A. Sarychev, "Electromagnetic properties of composites containing elongated conducting inclusions," Phys. Rev. B **53**, 6318–6336 (1996).
[35]M. Staffaroni, J. Conway, S. Vedantam, J. Tang, and E. Yablonovitch, "Circuit analysis in metal-optics," Photonics Nanostruct. Fundam. Appl. **10**, 166–176 (2012).
[36]P. B. Johnson and R. W. Christy, "Optical constants of the noble metals," Phys. Rev. B **6**, 4370–4379 (1972).
[37]S. I. Bozhevolnyi and T. Søndergaard, "General properties of slow-plasmon resonant nanostructures: Nano-antennas and resonators," Opt. Express **15**, 10869 (2007).
[38]L. Novotny, "Effective wavelength scaling for optical antennas," Phys. Rev. Lett. **98**, 266802 (2007).